

# Optical photometry and spectroscopy of the accretion-powered millisecond pulsar HETE J1900.1–2455

P. Elebert,<sup>1\*</sup> P. J. Callanan,<sup>1</sup> A. V. Filippenko,<sup>2</sup> P. M. Garnavich,<sup>3</sup> G. Mackie,<sup>4</sup> J. M. Hill<sup>5</sup> and V. Burwitz<sup>6</sup>

<sup>1</sup>*Department of Physics, University College Cork, Cork, Ireland*

<sup>2</sup>*Astronomy Department, University of California, Berkeley, CA 94720–3411, USA*

<sup>3</sup>*Department of Physics, University of Notre Dame, Notre Dame, IN 46556–5670, USA*

<sup>4</sup>*Centre for Astrophysics and Supercomputing, Swinburne University of Technology, Hawthorn, Victoria 3122, Australia*

<sup>5</sup>*Large Binocular Telescope Observatory, University of Arizona, Tucson, AZ 85721–0065, USA*

<sup>6</sup>*Max-Planck-Institut für extraterrestrische Physik, Giessenbachstraße, D-85741 Garching, Germany*

2 February 2008

## ABSTRACT

We present phase resolved optical photometry and spectroscopy of the accreting millisecond pulsar HETE J1900.1–2455. Our *R*-band light curves exhibit a sinusoidal modulation, at close to the orbital period, which we initially attributed to X-ray heating of the irradiated face of the secondary star. However, further analysis reveals that the source of the modulation is more likely due to superhumps caused by a precessing accretion disc. Doppler tomography of a broad  $H\alpha$  emission line reveals an emission ring, consistent with that expected from an accretion disc. Using the velocity of the emission ring as an estimate for the projected outer disc velocity, we constrain the maximum projected velocity of the secondary to be  $200 \text{ km s}^{-1}$ , placing a lower limit of  $0.05 M_{\odot}$  on the secondary mass. For a  $1.4 M_{\odot}$  primary, this implies that the orbital inclination is low,  $\lesssim 20^{\circ}$ . Utilizing the observed relationship between the secondary mass and orbital period in short period cataclysmic variables, we estimate the secondary mass to be  $\sim 0.085 M_{\odot}$ , which implies an upper limit of  $\sim 2.4 M_{\odot}$  for the primary mass.

**Key words:** accretion, accretion discs – techniques: photometric – techniques: spectroscopic – pulsars: individual: HETE J1900.1–2455 – X-rays: binaries

## 1 INTRODUCTION

Low mass X-ray binaries (LMXBs) are close binary systems consisting of a degenerate primary – black hole or neutron star (NS) – accreting matter from a low mass ( $< 1 M_{\odot}$ ) secondary, via Roche lobe overflow. X-ray transients (XRT) are LMXBs which undergo periodic outbursts, explained by the disc instability model (e.g. Dubus, Hameury & Lasota 2001), while persistently bright systems are permanently in the outbursting state. One subclass of LMXBs are the accretion-powered millisecond pulsars (AMSPs), the first of which, SAX J1808.4–3658, was discovered in 1998 (Wijnands & Van der Klis 1998). Seven more of these systems have been discovered since then (Poutanen 2006; Wijnands 2006; Markwardt, Krimm & Swank 2007).

In general, the outburst duration for AMSPs ranges from a few weeks to months. AMSPs generally contain a

weakly magnetized ( $\sim 10^8$ – $10^9$  G) NS with spin frequencies between 180 and 600 Hz. The orbital periods range between 40 min and 5 h. The secondary star in these systems is either a white or brown dwarf (Falanga et al. 2007, and references therein). Falanga et al. (2005) have measured the predicted decrease in the NS spin period for the AMSP system IGR J00291+5934, supporting the idea that these AMSPs are in fact old NS, which have over time been spun up to millisecond periods by acquiring angular momentum from the accretion of material from the secondary. As such, they provide the missing link between LMXBs and old, isolated millisecond radio pulsars.

In comparison to brighter LMXBs, relatively little is known about the optical properties of AMSPs. Even in outburst, the eight so far discovered are comparatively faint, the brightest being SAX J1808.4–3658 at  $R \simeq 16.2$  mag (Wang et al. 2001). In quiescence, these systems are generally very faint optically, the brightest measured again being SAX J1808.4–3658 at  $R \simeq 20.9$  mag.

\* E-mail: p.elebert@ucc.ie

HETE J1900.1–2455 is the seventh AMSP, discovered by Vanderspek et al. (2005) on 2005 June 14 by the *High Energy Transient Explorer II* (HETE II). Several type-I bursts have since been observed, and assuming that the peak flux observed during the brightest of these is Eddington-limited, HETE J1900.1–2455 is at a distance of  $\sim 4.3$  kpc (Suzuki et al. 2007).

The pulsation frequency was determined with the *Rossi X-ray Transient Explorer* to be 377.3 Hz (Morgan, Kaaret & Vanderspek 2005). Pulse timing analysis by Kaaret et al. (2006) revealed a circular orbit with a period ( $P_{\text{orb}}$ ) of  $\sim 83.3$  minutes ( $4995.258 \pm 0.005$  s), and a projected primary semimajor axis,  $a_1 \sin i$ , of  $18.41 \pm 0.01 \times 10^{-3}$  light second. These parameters combine to provide a mass function  $f(M) = 2.004 \pm 0.003 \times 10^{-6} M_{\odot}$ . Galloway et al. (2006) report that pulses were detected intermittently in the first two months after discovery. No pulses have been reported since then.

Unusually for an XRT, this system has remained active for more than 2 years, at a level of  $\sim 2 \times 10^{36}$  erg s $^{-1}$ . Several times during 2007 March/February, the X-ray flux fell by an order of magnitude, but each time returned to outburst levels within  $\sim 1$  week (Galloway et al. 2007). In 2007 May, the source was observed to decline to its lowest level since discovery (by a factor of  $> 10^3$ ), lasting for several weeks, prompting speculation that HETE J1900.1–2455 was returning to quiescence (Degenaar et al. 2007a; Galloway et al. 2007; Torres et al. 2007). However, the system returned to its outburst state within  $\sim 2$ –3 weeks (Degenaar et al. 2007b; Garnavich et al. 2007).

The optical counterpart was found by Fox (2005) with an *R*-band magnitude of  $\sim 18.4$  mag. Subsequent observations by Steeghs et al. (2005) found the *R*-band magnitude to be  $18.02 \pm 0.03$  mag, and the *V* – *R* colour (dereddened) to be  $-0.16$  mag, with spectroscopy revealing a broad He II  $\lambda 4686$  Å emission line.

In this paper we present optical photometry and spectroscopy of HETE J1900.1–2455 in its outburst state. These observations were motivated by several goals, key amongst them the aim of measuring the radial velocity of the secondary, and hence constraining the mass of the compact object. For the longer period transient systems, such measurements are possible via radial velocity studies of absorption lines from the secondary once the system has returned to quiescence. For the shorter period AMSPs however, the secondary is likely to be so faint as to make such observations extremely difficult, if not impossible. However, Steeghs & Casares (2002) and Casares et al. (2004) have shown how radial velocity measurements of the secondary are still possible for X-ray bright systems, by studying the Bowen blend emission from the irradiated face of the secondary: this technique may offer the only way of measuring the velocity of the secondary in AMSPs (i.e. whilst they are still X-ray bright), and usefully constraining the mass of the neutron star.

## 2 DATA

Our data consist of photometry obtained with the 2.3 m Advanced Technology Telescope (ATT) at Siding Spring Obser-

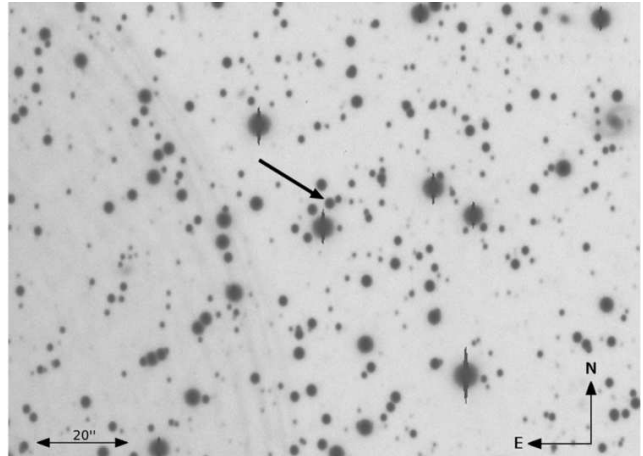


**Figure 1.** LBT image of the field of HETE J1900.1–2455 (Sloan *r*-band),  $2.3 \times 1.6$ . The black arrow indicates the position of HETE J1900.1–2455.

vatory, Australia, the 3.5 m Wisconsin-Indiana-Yale-NOAO (WIYN) telescope at Kitt Peak, Arizona, and the 8.4 m Large Binocular Telescope (LBT) at Mount Graham, Arizona. Our spectroscopy was obtained using the High Resolution Échelle Spectrometer (HIRES) on the 10 m Keck I telescope at Mauna Kea, Hawaii.

### 2.1 Photometry

We obtained photometry on 2 nights in 2006 September with the 2.3 m ATT, using the CCD4240 e2v detector, mounted at the  $f/18$  Nasmyth focus. The detector has  $2148 \times 2148$   $13.5 \mu\text{m}$  pixels, with  $0.34 \text{ pixel}^{-1}$ . On 2006 September 21 UT, we obtained 16 *R*-band exposures, covering slightly more than 1 orbital period, with exposure times of 60 s ( $\times 1$ ), 300 s ( $\times 9$ ) and 240 s ( $\times 6$ ). On the following night, we obtained *R*, *V* and *B*-band exposures,  $2 \times 300$  s exposures of each. On both nights, exposures were taken of the photometric standard field SA-112 (Landolt 1992). Seeing was  $\sim 2''$  on both nights, but deteriorated towards the end of the second night.

Three 300 s *R*-band exposures were also taken with the 3.5 m WIYN telescope on 2006 September 19 UT, using the WIYN Mini-Mosaic Imager, consisting of 2 SiTe CCDs, each with  $4096 \times 2048$   $15 \mu\text{m}$  pixels, with  $0.14 \text{ pixel}^{-1}$ . The seeing was  $\sim 2''$  for all 3 exposures. Exposures were also taken of the standard star field PG031+051 (Landolt 1992).

After the decline/rebrightening episode of 2007 May/June, we obtained additional observations using the LBT. On 2007 June 13 UT and June 24 UT we obtained 200 s Sloan *r*-band exposures of HETE J1900.1–2455 with the Large Binocular Camera (Blue) (Giallongo et al., in preparation; Ragazzoni et al. 2006) at the prime focus of the LBT (20 exposures per night). The eev-blue detector consists of 4 CCDs with  $2048 \times 4608$   $13.5 \mu\text{m}$  pixels, with  $0.224 \text{ pixel}^{-1}$ . The seeing on 2007 June 13 was  $\sim 0.85$ – $1.15''$ , while on June 24 was  $\sim 1''$ – $1.5''$ . The HETE J1900.1–2455 field is shown in Fig. 1 (from LBT on 2007 June 13, with seeing  $\sim 0.85''$ ).

All the photometry data were reduced in the same way. The frames were firstly bias corrected, trimmed and flat-

fielded using the CCDPROC routines in IRAF<sup>1</sup>. Photometry was performed using the DAOPHOT (Stetson 1992) point spread function fitting package in IRAF. The magnitude of HETE J1900.1–2455 was measured relative to several bright stars. These relative magnitudes were then calibrated by comparison with the standard star frames. Note that the WIYN data was used for photometric calibration only.

The ATT data from 2006 September gives  $R = 17.91 \pm 0.05$  mag,  $V = 18.00 \pm 0.04$  mag and  $B = 17.92 \pm 0.04$  mag. The errors quoted are an estimate of the systematic uncertainty. We note that the measured  $R$ -band magnitude is consistent with that reported by Steeghs et al. (2005). On 2007 June 13,  $R = 18.51 \pm 0.05$  mag, while on 2007 June 24,  $R = 18.44 \pm 0.05$  mag.

Taking the value for the hydrogen column density to the source,  $N_H$ , as  $1.6 \pm 0.4 \times 10^{21} \text{ cm}^{-2}$  (Campana, Cucchiara & Burrows 2005), and using the method detailed by Savage & Mathis (1979) yields  $E(B - V) = 0.30 \pm 0.08$ . The resulting dereddened colours are  $(B - V)_0 = -0.34 \pm 0.08$  mag, and  $(V - R)_0 = -0.17 \pm 0.06$  mag (again, consistent with the value reported by Steeghs et al. 2005).

In the  $R$ -band, HETE J1900.1–2455 is blended with a faint star 2'' to the northwest (see Fig. 1). This star was fitted simultaneously with HETE J1900.1–2455, and was found to have an  $R$ -band magnitude of  $20.1 \pm 0.1$  mag, which was constant, within these errors, in all our observations. This star was not visible in the  $B$  or  $V$ -band frames. This is consistent with the observations of Steeghs et al. (2005), who note that this blended star is  $\sim 2$  magnitudes fainter (in the  $R$ -band) than HETE J1900.1–2455.

In the LBT data, in frames with good seeing, an additional faint star is observed  $\sim 1''$  northwest of HETE J1900.1–2455, with an  $R$ -band magnitude  $\sim 5$  mag fainter than HETE J1900.1–2455.

In Fig. 2 we plot the three  $R$ -band light curves, folded on the pulse timing ephemeris of Kaaret et al. (2006). The phase error at the epochs of these optical observations, extrapolated from the error in the period of the pulse timing ephemeris, is  $\sim 0.01$ . Each light curve exhibits a similar modulation, but that of 2007 June 24 has an amplitude  $\sim 3$  times greater than for the other two. Clearly, the phasing of the three light curves is not consistent, implying that the period of this modulation is different to the orbital period.

## 2.2 Spectroscopy

Our spectroscopy was obtained using the HIRES spectrometer (Vogt et al. 1994) at the right Nasmyth focus of the 10 m Keck I telescope, with a  $52.68 \text{ lines mm}^{-1}$  échelle grism and the HIRESr 250  $\text{lines mm}^{-1}$  long wavelength cross disperser. The slit width was  $0.''86$  with a slit length of  $7''$ . The échelle grating angle was  $0^\circ$  and the cross disperser grating angle was  $0.^\circ 2405$ , providing a wavelength coverage of  $\sim \lambda\lambda 3900\text{--}8500 \text{ \AA}$ , spread over a mosaic of 3 MIT-Lincoln Labs CCDs (“red”, “green” and “blue”), each with  $2048 \times 4096 \text{ } 15 \mu\text{m}$

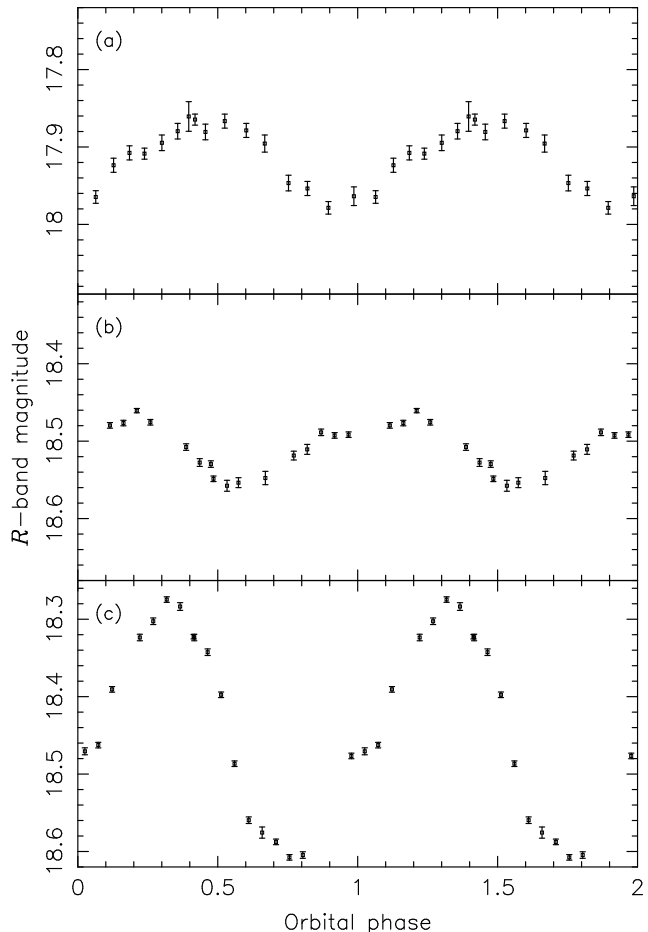


**Figure 2.**  $R$ -band light curves, folded on the pulse timing ephemeris (Kaaret et al. 2006), and plotted twice for clarity. (a) ATT light curve from 2006 September 21, (b) LBT light curve from 2007 June 13, (c) LBT light curve from 2007 June 24.

pixels, with  $0.''12 \text{ pixel}^{-1}$  in the spatial dimension. The images were binned by 2 pixels in the spatial dimension.

15 échelle spectra were obtained with HIRES on 2006 October 11 UT. Appropriate bias, flat, trace star, ThAr arc-clamp and flux standard (G191B2B) exposures were also taken. The object exposure times were 300 s ( $\times 5$ ), 360 s ( $\times 8$ ) and 420 s ( $\times 2$ ), with the 15 spectra covering slightly more than one orbital period.

The spectra were extracted using the MAKEE<sup>2</sup> (MAuna Kea Échelle Extraction) HIRES reduction package, which takes the two dimensional raw FITS images, and produces optimally extracted, wavelength calibrated, one dimensional spectra. The lines of interest to us were on the “blue” and “green” CCDs. The wavelength calibration was performed using the ThAr arc lamp exposures, by fitting a sixth order polynomial to an average of 30 lines per échelle order (minimum 20); this resulted in a dispersion of  $0.015\text{--}0.025 \text{ \AA pixel}^{-1}$  for the “blue” CCD and  $0.021\text{--}0.032 \text{ \AA pixel}^{-1}$  for the “green” CCD, and an RMS scatter of  $< 0.003 \text{ \AA}$  (average  $\sim 0.002 \text{ \AA}$ ). To confirm the extraction method implemented in MAKEE, the spectra were also extracted using the HIRES

<sup>1</sup> IRAF is distributed by the National Optical Astronomy Observatories, which are operated by the Association of Universities for Research in Astronomy, Inc., under cooperative agreement with the National Science Foundation.

<sup>2</sup> <http://spider.ipac.caltech.edu/staff/tab/makee/>

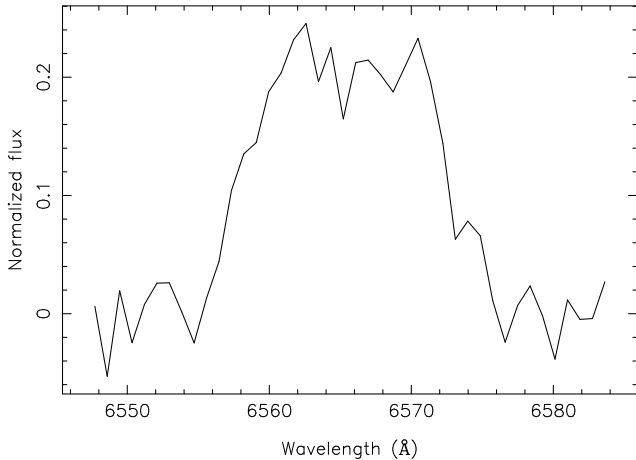


**Figure 3.** Average spectrum for  $H\alpha$ , normalized to the local continuum.

REDUX software<sup>3</sup>, and the ECHELLE package in IRAF: however the spectra extracted using all three methods were very similar.

The main emission features present in our spectra are  $H\alpha$   $\lambda 6563$  Å, He II  $\lambda 4686$  Å and the Bowen blend of N III and C III lines centred at  $\sim \lambda 4640$  Å.  $H\beta$  is present as a weak emission line within a broader absorption feature. The échelle orders containing these features were exported for further processing with the MOLLY spectroscopic data analysis package, and DOPPLER, a package used for performing maximum entropy Doppler tomography. The spectra were re-binned onto a velocity scale of  $40 \text{ km s}^{-1} \text{ pixel}^{-1}$ , yielding a signal-to-noise (S/N) ratio of  $6\text{--}16 \text{ pixel}^{-1}$ . The S/N varied across each order, particularly on the “blue” CCD, with the lowest S/N near the edges of the orders. For each spectrum, the continuum was fitted with a 2nd order polynomial, after masking the emission regions. The fit was then divided into the spectrum, and the remaining continuum subtracted. The average processed spectrum for  $H\alpha$  is shown in Fig. 3, and that for the Bowen blend and He II  $\lambda 4686$  Å is in Fig. 4. Note that the data in Fig. 4 has been boxcar smoothed, and shifted to the rest frame of the system. From the averaged spectra, the equivalent width for  $H\alpha$  is  $-3.1 \pm 0.3$  Å, for He II  $\lambda 4686$  Å is  $-2.5 \pm 0.3$  Å, and for the Bowen blend is  $-2.1 \pm 0.2$  Å. This is in contrast to the observations of Steeghs et al. (2005), who report that although their spectroscopy was contaminated by a nearby star, the main feature observed was a broad emission line from He II  $\lambda 4686$  Å and Balmer emission was at most very weak.

### 3 RESULTS

#### 3.1 R-band Light Curves

The three light curves in Fig. 2 exhibit a sinusoidal modulation, classically attributed to X-ray irradiation of the inner face of the secondary, where the modulation is due to the phase dependent visibility of this higher temperature region.

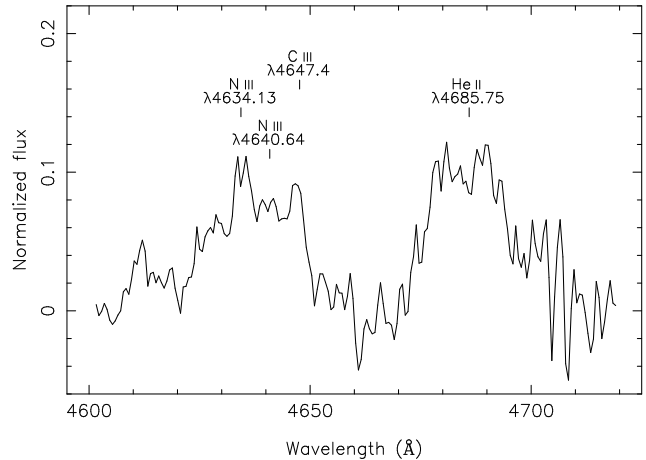


**Figure 4.** Average spectrum for the Bowen blend and He II  $\lambda 4686$  Å, normalized to the local continuum. The spectrum has been shifted to the rest frame of the system, based on the systemic velocity determined from the  $H\alpha$  emission line in section 3.2. The spectrum has also been boxcar smoothed.

The phasing of the ATT light curve is approximately consistent with this scenario, with the brightest measurements occurring near phase 0.5. However, the phasing of the other light curves is completely different, suggesting that the observed modulation does not vary on the orbital period. In particular, the two LBT light curves are separated by only 11 nights, and in that time the phasing of the light curves, folded on the orbital period, differs by  $\sim 0.2$ .

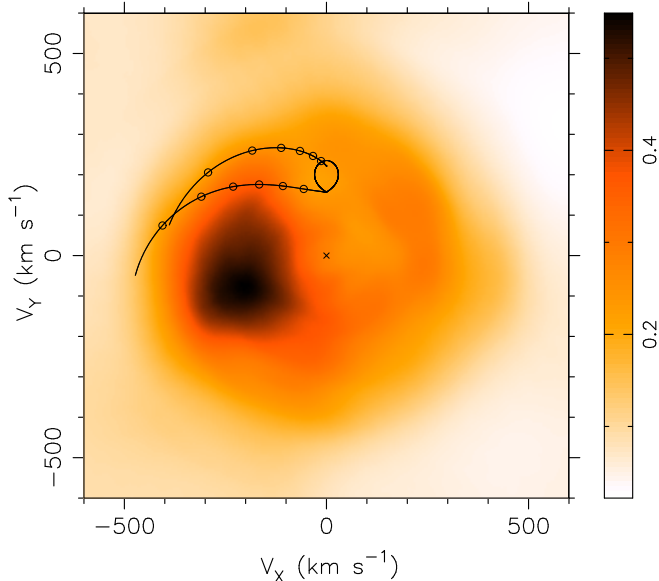
#### 3.2 $H\alpha$ emission

Fig. 3 shows the average  $H\alpha$  spectrum. This broad emission line exhibits a hint of a double peak (a classic signature of an accretion disc), although the peaks are not as distinctive as those seen in the spectra of other LMXBs. The distribution of the flux appears to be symmetrical about a central wavelength, suggesting that, on average, the emission from the disc is axisymmetrical. To constrain the systemic velocity,  $\gamma$ , we fitted a Gaussian to the wings of the averaged spectrum, where the emission is from disc regions closer to the centre, and presumably less susceptible to corruption from the hotspot and other non-uniformities in the outer disc (Marsh 1998). This gives a value for  $\gamma$  of  $132 \pm 8 \text{ km s}^{-1}$ .

We investigated the emission line distribution of the system by examining a Doppler tomogram of the  $H\alpha$  line (Fig. 5), constructed using  $\gamma = 132 \text{ km s}^{-1}$ . As with the photometry, the spectra were phased using the pulse timing ephemeris. For this work, we used the maximum entropy method, implemented in DOPPLER: see Marsh and Horne (1988), Marsh (2001) and Steeghs (2004) for further details and applications of Doppler tomography.

Enhanced emission is present in the  $(-V_x, +V_y)$  quadrant, extending into the  $(-V_x, -V_y)$  quadrant, with a faint ring of emission. Such a ring of emission is seen in Doppler tomograms of many LMXBs, and is attributed to emission from the outer disc (Marsh 1998). This emission ring lies between radii of  $\sim 200\text{--}400 \text{ km s}^{-1}$ . Plotting only the axisymmetric component of this tomogram reveals that the brightest emission is from an annulus at a velocity of  $\sim 230$

<sup>3</sup> <http://www.icolick.org/~xavier/HIRedux/>



**Figure 5.** Doppler tomogram for H $\alpha$ . The Roche lobe of the secondary is plotted. The lower curve represents the gas stream velocity (the free-fall ballistic trajectory from the inner Lagrangian point,  $L_1$ ) and the upper curve is the Keplerian velocity of the accretion disc along the gas stream. Both curves are marked with a circle when the gas stream moves  $0.1R_{L1}$  (0.1 of the distance between the primary and  $L_1$ ) closer to the primary. The gas stream trajectory and disc velocity along the stream were calculated using  $K_2 = 200 \text{ km s}^{-1}$  and  $q = 0.035$ .

$\text{km s}^{-1}$ , but with significant emission extending to  $\sim 150 \text{ km s}^{-1}$ . Since the secondary must be moving slower than the outer disc, we choose  $200 \text{ km s}^{-1}$  as an upper limit to  $K_2$ , the velocity of the secondary projected onto the line of sight.

For illustration, we plot in Fig. 5 the Roche lobe of the secondary, the gas stream trajectory and accretion disc velocity curve, computed using  $K_2 = 200 \text{ km s}^{-1}$ . Since  $K_1$  is already accurately known from the pulse timing analysis ( $2\pi a_1 \sin i / P_{\text{orb}} = 6.942 \pm 0.003 \text{ km s}^{-1}$ ; Kaaret et al. 2006),  $q$  ( $\equiv K_1/K_2$ ) = 0.035.  $K_2$  and  $q$  are the only parameters upon which the locations of the Roche lobe and the gas stream trajectory depend. At this value of  $K_2$ , the predicted gas stream misses the hotspot location. Lower values of  $K_2$  would cause the gas stream to be closer to the hotspot. However, we also note that Doppler tomograms of the He II  $\lambda 4686 \text{ \AA}$  emission line in the two NS LMXBs V801 Ara and V926 Sco also show the peak of emission in the  $(-V_x, -V_y)$  quadrant, close to the  $-V_x$  axis, and for these systems this emission is attributed to an extended disc bulge (Casares et al. 2006). As will be discussed in section 4, the location of the hotspot in HETE J1900.1–2455 may be explained by a warped, irradiated accretion disc.

### 3.2.1 Projected secondary velocity vs. inclination

Using the standard mass function equation, and with  $K_2 = K_1/q = 2\pi a_1 \sin i / q P_{\text{orb}}$  it is possible to calculate  $q$  and  $K_2$  for various orbital inclinations ( $i$ ) and primary masses ( $M_1$ ).

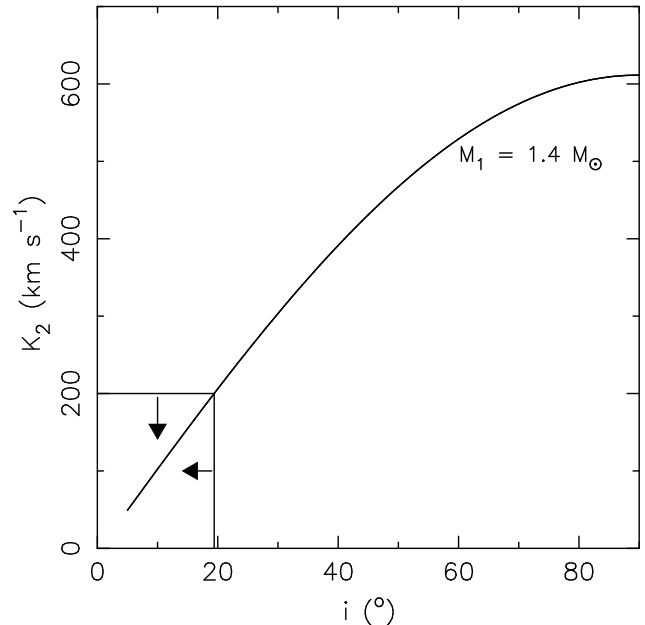


**Figure 6.** Projected secondary velocity ( $K_2$ ) vs. orbital inclination angle ( $i$ ) for a primary mass of  $1.4 M_{\odot}$ . The upper limit on  $K_2$  is set by the velocity of the H $\alpha$  emission ring.

Fig. 6 shows a plot of  $K_2$  vs.  $i$  for a primary mass of  $1.4 M_{\odot}$ . If  $K_2 < 200 \text{ km s}^{-1}$ ,  $i \lesssim 20^\circ$ , for all  $M_1 > 1.4 M_{\odot}$ .

Hence our upper limit on  $K_2$  provides an upper limit on  $i$  of  $\sim 20^\circ$ . This low inclination is consistent with the fact that the double peak in H $\alpha$  is not as clear as in systems with higher inclinations, and thus higher projected disc velocities (see for example the LMXB XTE J1118+480, with  $i \sim 70^\circ$ ; Elebert, Callanan & Torres 2006).

### 3.3 Bowen blend emission

Steehgs & Casares (2002) discovered that emission from the Bowen blend (a blend of N III, C III and O II lines, centred at  $\sim 4640 \text{ \AA}$ ) traced the motion of the irradiated secondary star in the LMXB Sco X-1. Some of the major features seen in the Bowen blend in X-ray binaries are the N III lines at  $\lambda 4634.13 \text{ \AA}$ ,  $\lambda 4640.64 \text{ \AA}$  and  $\lambda 4641.85/4641.96 \text{ \AA}$ , and the C III lines at  $\lambda 4647.4 \text{ \AA}$ ,  $\lambda 4650.1 \text{ \AA}$  and  $\lambda 4651 \text{ \AA}$  (Hynes et al. 2001; Steeghs & Casares 2002; Nelemans, Jonker & Steeghs 2006). Our average spectrum of the Bowen blend reveals a broad range of emission between  $\lambda 4620 \text{ \AA}$  and  $\lambda 4650 \text{ \AA}$  (Fig. 4). Superimposed on this broad emission, there appear to be several narrower emission features, three of which correspond to the expected wavelengths of the N III  $\lambda 4634.13 \text{ \AA}$  line, the N III blend near  $\lambda 4641 \text{ \AA}$ , and the  $\lambda 4647.4 \text{ \AA}$  C III line.

Because of the low S/N, we performed Doppler tomography of all of the lines in the Bowen blend simultaneously, with the intention of finding emission from the irradiated face of the secondary. Although this map contains a single sharp spot of emission, it is in the  $(+V_x, +V_y)$  quadrant,  $\sim 45^\circ$  away from the expected location of secondary emission on the  $+V_y$  axis. The significance of this emission is uncertain because of the low S/N of the individual exposures.

### 3.4 He II $\lambda 4686$ Å emission

The He II  $\lambda 4686$  Å emission is contaminated in the wings, particularly on the red side. While the lower S/N in the wings might explain some of this variability, it does not account for all of the systematic artefacts seen – in particular, the 2 dips on the red side, near  $\lambda 4704$  Å and  $\lambda 4710$  Å, can be seen in averages of just a few spectra, and so are not due to random noise. As well as this, the average line appears asymmetrical, with an excess of flux between  $\lambda\lambda 4695$ – $4705$  Å. The S/N ratio throughout the order is also lower than that for H $\alpha$ . Despite this, a Gaussian fit to the wings of this line (masking the line core, and the excess on the red side) gives a systemic velocity consistent with that seen in the H $\alpha$  emission.

## 4 DISCUSSION

With its maximum brightness near phase 0.5, we attempted to fit the first of our light curves (Fig. 2(a)) using the Eclipsing Light Curve (ELC) code (Orosz & Hauschildt 2000), under the assumption that the modulation was due to X-ray heating. This provided a satisfactory fit, although because of the degeneracy between inclination angle, disc temperature and disc flaring angle, it was not possible to extract a unique parameter set, and a wide range of parameter values yielded equally good fits.

However, the phasing of the subsequent light curves (Fig. 2(b),(c)) suggests that the observed modulation is not due to X-ray heating of the secondary: the most likely explanation for this is that the observed modulation is due to superhumps (see below). Therefore the apparent alignment of the first light curve is most likely coincidental, and the ELC code (which does not incorporate superhumps) cannot be used to extract reliable system parameters.

Superhumps are periodic optical modulations, originally seen during superoutbursts of SU UMa dwarf novae (DNe), but also seen in some LMXBs in outburst (Haswell et al. 2001a, and references therein). The phenomenon has also been seen in persistently bright systems. The superhump period is typically a few percent longer than  $P_{\text{orb}}$ . The current understanding is that in systems where the mass ratio is less than  $\sim 0.25$ , the tidal truncation radius lies outside the 3:1 resonance radius. When the accretion disc radius extends out to beyond the 3:1 resonance radius, the disc becomes eccentric, and the perturbation from the secondary causes a prograde precession. For precessing discs in LMXBs, Haswell et al. (2001a) proposed that the disc area changes on the superhump period, causing the area of the disc intercepting the X-rays to increase. The increased reprocessing causes the disc to brighten, giving rise to the observed superhumps in LMXBs. Several systems exhibit superhumps with almost exact sinusoidal modulations like those seen in HETE J1900.1–2455, in particular another LMXB, XTE J1118+480 (Patterson et al. 2005). The peak-to-peak amplitude of the modulation seen in HETE J1900.1–2455 was  $\sim 0.1$  mag on 2006 September 21 and 2007 June 13, but increased to  $\sim 0.3$  mag on 2007 June 24. The latter amplitude is quite high, but as pointed out by Haswell et al. (2001b) superhumps due to irradiated discs are likely to appear more prominent at *low* inclinations:

hence the large superhump amplitude supports our estimate of the inclination in section 3.2.1. For an X-ray luminosity of  $\sim 10^{36}$  erg s $^{-1}$  the disc is likely to also suffer irradiation-driven warping (Foulkes, Haswell & Murray 2006, in particular their model number 1) and the disc shape continuously changes under the combination of prograde apsidal precession and retrograde warped precession. Such models may also explain the factor of  $\sim 3$  increase in modulation amplitude over a relatively short timescale (Haswell, private communication).

The location of the hotspot in the H $\alpha$  Doppler tomogram may be interpreted in terms of this irradiated precessing disc model: as the warped disc precesses, the gas stream/accretion disc impact point varies. How this occurs can be seen clearly in the Foulkes, Haswell & Murray (2006) simulations<sup>4</sup>. These simulations suggest that multi-epoch Doppler tomography of HETE J1900.1–2455 should reveal a hotspot whose location varies between the  $(-V_x, +V_y)$  and  $(-V_x, -V_y)$  quadrants.

Previous work has shown that, once the superhump period ( $P_{\text{sh}}$ ) is identified, then the period excess,  $\epsilon$  ( $= (P_{\text{sh}} - P_{\text{orb}})/P_{\text{orb}}$ ), can be directly related to the mass ratio (Patterson et al. 2005). A Fourier transform of our photometry, however, does not allow us to identify a unique superhump period, because our sampling is too sparse. A more comprehensive photometry campaign is required to measure  $P_{\text{sh}}$ , and estimate  $q$ .

Using the empirical relationship between the absolute visual magnitude of an irradiated accretion disc ( $M_v$ ), the X-ray luminosity of the central source and orbital period (van Paradijs & McClintock 1994; de Jong, van Paradijs & Augusteijn 1996), we find  $M_v = 3.6 \pm 0.5$  mag. At a distance of 4.3 kpc (Suzuki et al. 2007), such a disc should have an apparent magnitude of  $16.7 \pm 0.5$  mag. This is consistent with the measured V-band magnitude of  $\sim 17.1$  mag, implying that the optical light, in the V-band, is dominated by an X-ray heated accretion disc. Thus, X-ray heating of the disc can explain the observed optical brightness of HETE J1900.1–2455.

Kaaret et al. (2006) estimated the mass of the secondary to be between 0.016 and 0.07  $M_{\odot}$ , for primary masses between 1.4 and 2.2  $M_{\odot}$ , but this was based on an assumption of inclination angle:  $90^\circ$  for the lower mass limit, and a uniform a priori distribution for the 95 per cent confidence upper limit. We have seen that for  $K_2 < 200$  km s $^{-1}$ ,  $i \lesssim 20^\circ$  (see Fig. 6). At this upper limit of  $K_2$ ,  $q = 0.035$ , and the minimum value of  $M_2$  (for  $M_1 = 1.4 M_{\odot}$ ) is therefore 0.05  $M_{\odot}$ .

Patterson et al. (2003) have computed a mass-radius relation for the secondaries in short period cataclysmic variables (CVs), finding that in general, the mass-radius curve lies above that for zero-age main sequence stars. An empirical equation relates  $M_2$  to  $P_{\text{orb}}$ :  $M_2 = 0.0764 P_{\text{orb}}^{1.37} \alpha^{-2.05} M_{\odot}$ , where  $\alpha$  is the factor relating the radius of the secondaries in these CVs to that of main sequence stars with the same mass, and  $P_{\text{orb}}$  is in hours. Patterson et al. (2003) find that  $\alpha \simeq 1.18$ . Assuming that the secondary in HETE J1900.1–2455 is similar to the secondary in these CV systems, this equation predicts  $M_2 =$

<sup>4</sup> [http://physics.open.ac.uk/FHM\\_warped\\_disc/q0p075.avi](http://physics.open.ac.uk/FHM_warped_disc/q0p075.avi)

0.085  $M_{\odot}$ . With the lower limit on  $q$  of 0.035, this sets an upper limit to the primary mass of  $M_1 < 2.4 M_{\odot}$ . The secondary may also be a brown dwarf, in which case  $M_2$  is poorly constrained, as is  $M_1$ .

Finally, we briefly examine the radial velocity of HETE J1900.1–2455 relative to the local Galactic radial velocity. Based on its position and estimated distance, HETE J1900.1–2455 is  $\sim 3.6$  kpc from the Galactic centre,  $\sim 1$  kpc below the Galactic plane. Using the Galactic rotation curve of Clemens (1985), we find that the radial velocity of HETE J1900.1–2455 is  $\sim 90$  km s $^{-1}$  relative to the local Galactic rotation. Combined with future proper motion studies, this velocity may be used to derive the space velocity of HETE J1900.1–2455 and compute its orbit around the Galactic Centre (e.g. Mirabel & Rodrigues 2003).

## 5 CONCLUSIONS

We have presented a detailed optical study of the AMSP HETE J1900.1–2455. The  $R$ -band light curves reveal a modulation whose phase is inconsistent with simple heating of the secondary star/accretion disc: we interpret this as due to superhumps associated with a precessing accretion disc. Fitting to the wings of the averaged H $\alpha$  emission line gives the systemic velocity of  $132 \pm 8$  km s $^{-1}$ , and a similar value is found from the He II line.

Doppler tomography of the H $\alpha$  emission line suggests a upper limit of  $\sim 200$  km s $^{-1}$  on the projected secondary velocity, implying that HETE J1900.1–2455 has a low inclination,  $\lesssim 20^\circ$ , and a minimum secondary mass of  $0.05 M_{\odot}$ .

Assuming that the secondary in HETE J1900.1–2455 is similar to those seen in short period CVs, we estimate a secondary mass of  $0.085 M_{\odot}$ , which implies an upper limit to the NS mass of  $2.4 M_{\odot}$  (again for  $K_2 \lesssim 200$  km s $^{-1}$ ). If the secondary is a brown dwarf, then this constraint is relaxed.

## ACKNOWLEDGMENTS

We acknowledge the use of the 2.3 m Advanced Technology Telescope of the Australian National University at Siding Spring Observatory. The WIYN Observatory is a joint facility of the University of Wisconsin-Madison, Indiana University, Yale University, and the National Optical Astronomy Observatory. Some of the data presented herein were acquired using the Large Binocular Telescope (LBT). The LBT is an international collaboration among institutions in the United States, Italy and Germany. LBT Corporation partners are: The University of Arizona on behalf of the Arizona university system; Istituto Nazionale di Astrofisica, Italy; LBT Beteiligungsgesellschaft, Germany, representing the Max-Planck Society, the Astrophysical Institute Potsdam, and Heidelberg University; The Ohio State University, and The Research Corporation, on behalf of The University of Notre Dame, University of Minnesota and University of Virginia. We thank LBT director R. Green for allocation of DD time, and D. Thompson, LBTO for acquiring some of the data. The spectroscopic data presented herein were obtained at the W. M. Keck Observatory, which is operated as a scientific partnership among the California In-

stitute of Technology, the University of California and the National Aeronautics and Space Administration. The observatory was made possible by the generous financial support of the W. M. Keck Foundation. This research made use of NASA's Astrophysics Data System, and the SIMBAD database, operated at CDS, Strasbourg, France. X-ray quick-look results provided by the ASM/RXTE team. We acknowledge the use of MOLLY and DOPPLER software packages developed by T. R. Marsh, University of Warwick. We thank J. X. Prochaska, UCO/Lick Observatory, for reducing our Keck spectroscopy using HIRES REDUX. PE and PJC acknowledge support from Science Foundation Ireland.

## REFERENCES

- Campana S., Cucchiara A., Burrows D. N., 2005, ATel, 543
- Casares J., Steeghs D., Hynes R. I., Charles P. A., Cornelisse R., O'Brien K., 2004, RevMexAA Conference Series, 20, 21
- Casares J., Cornelisse R., Steeghs D., Charles P. A., Hynes R. I., O'Brien, K., Strohmayer, T. E., 2006, MNRAS, 373, 1235
- Clemens, D. P., 1985, ApJ, 295, 422
- Degenaar N., Wijnands R., Galloway D. K., Lewin W. H. G., Homan J., Chakrabarty D., Campana S., Miller J. M., Cackett E. M., 2007a, ATel, 1091
- Degenaar N., Campana S., Galloway D. K., Lewin W. H. G., Homan J., Chakrabarty D., Morgan E. H., Jonker P. G., Cackett E. M., Miller J. M., Wijnands R., 2007b, ATel, 1106
- de Jong J. A., van Paradijs J., Augusteijn T., 1996, A&A, 314, 484
- Dubus G., Hameury J.-M., Lasota J.-P., 2001, A&A, 373, 251
- Elebert P., Callanan P. J., Torres M. A. P., 2006, in Meurs E. J. A., Fabbiano G., Eds., Proceedings of the 230th Symposium of the International Astronomical Union, Cambridge University Press, pp. 57–58
- Falanga M., Kuiper L., Poutanen J., Bonning E. W., Di Salvo T., Goldoni P., Goldwurm A., Shaw S. E., Stella L., 2005, A&A, 444, 15
- Falanga M., Poutanen J., Bonning E. W., Kuiper L., Bonnet-Bidaud J. M., Goldwurm A., Hermsen W., Stella L., 2007, A&A, 464, 1069
- Foulkes S. B., Haswell C. A., Murray J. R., 2006, MNRAS, 366, 1399
- Fox D. B., 2005, ATel, 526
- Galloway D. K., Morgan E. H., Krauss M. I., Kaaret P., Chakrabarty D., 2006, ApJ, 654, L73
- Galloway D. K., Morgan E. H., Chakrabarty D., Kaaret P., 2007, ATel, 1086
- Garnavich P. M., Callanan P. J., Elebert P., Reynolds M. T., 2007, ATel, 1110
- Haswell C. A., King A. R., Murray J. R., Charles P. A., 2001a, MNRAS, 321, 475
- Haswell C. A., Rolfe D. J., King A. R., Murray J. R., Charles P. A., 2001b, ApSSS, 276, 41
- Hynes R. I., Charles P. A., Haswell C. A., Casares J., Zurita C., Serra-Ricart M., 2001, MNRAS, 324, 180
- Kaaret P., Morgan E. H., Vanderspek R., Tomsick J. A., 2006, ApJ, 639, 963

- Landolt A. U., 1992, *ApJ*, 104, 340
- Markwardt C. B., Krimm H. A., Swank J. H., 2007, *ATel*, 1108
- Marsh T. R., Horne K., 1988, *MNRAS*, 236, 269
- Marsh T. R., 1998, in Howell S., Kuulkers E., Woodward C., Eds., *ASP Conf. Ser. Vol. 137, Wild Stars in the Old West*, ASP, San Francisco, pp. 236–244
- Marsh T. R., 2001, in Boffin H. M. J., Steeghs D., Cuypers J., Eds., *Astrotomography: Indirect Imaging Methods in Observational Astronomy*, LNP Series 573, Springer, Berlin, pp. 1–26
- Mirabel I. F., Rodrigues I., 2003, *A&A*, 398, L25
- Morgan E. H., Kaaret P., Vanderspek R., 2005, *ATel*, 523
- Nelemans G., Jonker P. G., Steeghs D., 2006, *MNRAS*, 370, 255
- Orosz J. A., Hauschildt P. H., 2000, *A&A*, 364, 265
- Patterson J., Thorstensen J. R., Kemp J., Skillman D. R., Vanmunster T., Harvey D. A., Fried R. A., Jensen L., Cook L. M., Rea R., Monard B., McCormick J., Velthuis F., Walker S., Martin B., Bolt G., Pavlenko E., O'Donoghue D., Gunn J., Novák R., Masi G., Garradd G., Butterworth N., Krajci T., Foote J., Beshore E., 2003, *PASP*, 115, 1308
- Patterson J., Kemp J., Harvey D. A., Fried R. E., Rea R., Monard B., Cook L. M., Skillman D. R., Vanmunster T., Bolt G., Armstrong E., McCormick J., Krajci T., Jensen L., Gunn J., Butterworth N., Foote J., Bos M., Masi G., Warhurst P., 2005, *PASP*, 117, 1204
- Poutanen J., 2006, *AdSpR*, 38, 2697
- Ragazzoni R., Giallongo E., Pasian F., Baruffolo A., Bertram R., Diolaiti E., Di Paola A., Farinato J., Gentile G., Hill J., Lombini M., Pedichini F., Speziali R., Smareglia R., Vernet E., 2006, in Stepp, L. M., Ed., *Society of Photo-Optical Instrumentation Engineers (SPIE) Conference, Volume 6267, Ground-based and Airborne Telescopes*
- Savage B. D., Mathis J. S., 1979, *ARA&A*, 17, 73
- Steeghs D., 2004, *AN*, 325, 185
- Steeghs D., Casares J., 2002, *ApJ*, 568, 273
- Steeghs D., Torres M. A. P., Garcia M. R., McClintock J. E., Miller J. M., Jonker P. G., Callanan P. J., Zhao P., Berlind P., Hutchins R., Watson C., 2005, *ATel*, 543
- Stetson P. B., 1992, in Worrall D. M., Biemesderfer C., Barnes J., Eds., *Astronomical Data Analysis Software and Systems I*, *ASP Conf. Ser.*, 25, 297, pp. 297–306
- Suzuki M., Kawai N., Tamagawa T., Yoshida A., Nakagawa Y. E., Tanaka K., Shirasaki Y., Matsuoka M., Ricker G. R., Vanderspek R., Butler N., Lamb D. Q., Graziani C., Pizzichini G., Sato R., Arimoto M., Kotoku J., Maetou M., Yamauchi M., 2007, *PASJ*, 59, 263
- Torres M. A. P., Rodriguez-Gil P., Steeghs D., Corral-Santana J. M., Casares J., Jonker P. G., 2007, *ATel*, 1090
- Vanderspek R., Morgan E. H., Crew G., Graziani C., Suzuki M., 2005, *ATel*, 516
- van Paradijs J., McClintock J. E., 1994, *A&A*, 290, 133
- Vogt S. S., Allen S. L., Bigelow B. C., Bresee L., Brown B., Cantrall T., Conrad A., Couture M., Delaney C., Epps H. W., Hilyard D., Hilyard D. F., Horn E., Jern N., Kanto D., Keane M. J., Kibrick R. I., Lewis J. W., Osborne J., Pardeilhan G. H., Pfister T., Ricketts T., Robinson L. B., Stover R. J., Tucker D., Ward J., Wei M. Z., 1994, *SPIE*, 2198, 362
- Wang Z., Chakrabarty D., Roche P., Charles P. A., Kuulkers E., Shahbaz T., Simpson C., Forbes D. A., Helsdon S. F., 2001, *ApJ*, 563, L61
- Wijnands R., 2006, in Lowry, J. A., Ed., *Trends in Pulsar Research*, Nova Science Publishers, New York, pp. 53–78
- Wijnands R., van der Klis, M., 1998, *Nature*, 294, 344

This paper has been typeset from a  $\text{\LaTeX}$  file prepared by the author.